Investigation of cementitious materials subjected to aggressive environments exposure by means of SESANS : application to nuclear waste storage

by

D. Muller

in partial fulfillment of the requirements for the degree of

Bachelor of Science
in Applied Physics

at the Delft University of Technology,
to be defended publicly on Monday October 6, 2016 at 13:30 AM.

Supervisor:	Dr. A. Sabau	
Thesis committee:	Prof. dr. A. van Well,	TU Delft
	Prof. dr. W. Bouwman,	TU Delft
	Dr. D. Bykov,	TU Delft

TU Delft Delft University of Technology

Preface

I would like to thank Zhou Zhou and Evgeni for their help with the Matlab code and interpretation of the data. Next I would like to thank Wim Bouwman for the advice on choosing my model. I would like to thank Chris Duif for his help with the SESANS measurements. Last but not least I would like to thank Andrea Sabau and Denis Bykov for their guidance in my research project.

D. Muller
Delft, September 2016

Contents

List of Figures vii

1 Introduction 1

2 Spin Echo Small Angle Neutron Scattering 3
2.1 SESANS . . . 3
2.2 Fractal Geometry . . . 5
2.3 Infinitely long Cylinder with diameter D . . . 6

3 Scanning Electron Microscopy and X-ray Powder Diffraction 7
3.1 SEM . . . 7
3.2 Energy-dispersive X-ray spectroscopy (EDX) . . . 8
3.3 X-ray Powder Diffraction . . . 9

4 Overview of Geological Repository 11
4.1 Cementitious Materials . . . 11
4.1.1 Backfill concrete . . . 12
4.1.2 Conditioning concrete . . . 13

5 Experiments 15
5.1 Sample Preparation . . . 15
5.1.1 Cutting the Concrete Samples . . . 15
5.1.2 Degradation of the Concrete Samples . . . 15
5.2 Chemistry . . . 16

6 Analysis of SESANS 19
6.1 Visual Interpretation . . . 19
6.2 Surface Fractal Model . . . 22
6.3 Infinitely long Cylinder with diameter D . . . 23

7 Analysis of SEM, EDX and XRD 25

8 Conclusion and Recommendations 29

Bibliography 31

List of Figures

2.1 Schematic view of magnetic fields in SESANS 4
2.2 Interpretation of data in SESANS 5

3.1 Schematic view a Scanning Electron Microscope (SEM) 7
3.2 Sputter Coater: Quorum 300 8
3.3 Schematic view a X-ray Powder Diffraction (XRD) 10
3.4 Example of XRD 10

4.1 The proposed repository by OPERA 11
4.2 One gallery of the proposed repository by OPERA 12
4.3 200 liter drums 13

5.1 Carbonation chamber 17

6.1 Interpretation of data in SESANS 19
6.2 SESANS measurement of CEMI 20
6.3 SESANS measurements of CEMI 20
6.4 SESANS measurements of CEMIII 21
6.5 Transmission of CEMI samples 21
6.6 Transmission of CEMI samples 22
6.7 Test sample with surface fractal fit 22
6.8 Associated length visualization 23

7.1 SEM measurement of CEMI 25
7.2 SEM measurement of CEMI with length-scales of pores 26
7.3 SEM measurement of CEMIII/B 26
7.4 SEM measurement of CEMIII with length-scales of pores 26
7.5 EDX measurement of undegraded CEMI 27
7.6 EDX measurement of undegraded CEMIII 27
7.7 XRD pattern of CEMI degraded in sulphate solution for two weeks 28
7.8 XRD pattern of CEMIII/B carbonated for two weeks 28

1

Introduction

Boom Clay is considered as potential host rocks for disposal of radioactive waste in geological formation in Belgium and the Netherlands. Until now waste is collected and stored by COVRA ("Centrale Organisatie Voor Radioactief Afval"). This is for a period of at least 100 years. However, a big part of this waste is still radioactive after this period. In the meantime a research program called OPERA ("Onderzoeksprogramma Eindberging Radioactief Afval") is started in July 2011 to look for longtime storage in geological repositories.
The radioactive waste can be classified in three categories. Low- and Intermediate (LILW) Level Waste originates from a wide range of sources as operation of nuclear power plants [1]. LILW can also be divided into sub-categories giving information about their origin and the kind of emittance. LILW represents the biggest fraction of the total radioactive waste in the Netherlands. TE Norm 'Technically Enhanced Naturally Occurring Radioactive Material' consists only of depleted uranium from the enrichment facility URENCO. High Level Waste (HLW) is divided into heat generating and non-heat generating HLW. Heat generating HLW consists of spent fuel elements from High Flux Reactor in Petten and the "Hoger Onderwijs Reactor" in Delft. Non-heat generating HLW contain hulls and ends from Nuclear Power Plants (NPR) like in Borsele and waste from the decommissioning of nuclear facilities [2].
Clay is a very favorable granular material for disposing nuclear waste. It is a fine grained natural rock or soil material that combines one or more clay minerals with metal oxides and organic matter. A few advantages of clay are low permeability, low hydraulic gradient and high capacity to retard the migration of radio-nuclides towards the accessible environment. Most of the materials used in the repository is concrete and so we want to know if the concrete is affected by these aggressive chemicals, which are present in this environment.
For the mechanical support the gallery lining is provided during the constructional and operational phase of a geological disposal facility [3]. These concrete segments are proposed to be made with Portland cement. Enclosure of the waste is provided by the backfill, which is proposed to be made with foam concrete of Portland cement. Containment of waste is provided by the waste package, which is proposed to be made with Portland cement for HLW and depleted uranium. For LILW concrete made with blast furnace slag cement is proposed.
It is interesting to perform experiments to study the interface processes between the concrete and Boom clay for the impact on transport processes. This is part of the EU-research project called Cebama. In this research cement-based materials, properties, evolution, barrier functions interactions between the host rock (Boom clay) and cement are investigated. Boom clay contains minerals like pyrite and organic matter, both sensitive to oxidation. This way acidification can occur in the Boom clay, which has to be prevented for the durability of the concrete.
However, these reactions between the Boom Clay pore water and the concrete only occur over very long periods of time. The goal is to investigate the nano-porosity structure [4] of the concrete with SESANS (Spin Echo Small Angle Neutron Scattering), Scanning Electron Microscopy (SEM) and X-ray Powder Diffraction (XRD). The concrete (certified concrete for conditioning Low Level waste) is provisioned by COVRA. These samples will be immersed in aggressive chemical solutions to speed up the degradation process. However these concentrations are much lower than the concentrations used for the experiments. The reason for this is that at the actual concentrations no effect can be observed in

the given time limit of the project.
We want to look at these samples with use of SESANS. We use SESANS instead of SANS, because SESANS can measure samples over larger length scales 10-10000 nm instead of 1-100 nm. SESANS is a relatively new method to determine the structure of materials in real space. In this research experiments are performed at the Reactor Institute Delft. SESANS uses neutrons from the core of the nuclear reactor. The method is based on the Larmor precession of polarized neutrons transmitted through pi/2-flippers, before and after the sample. This encodes the scattering angle into a net precision angle. The goal is to measure these concrete samples (immersed in boom clay pore water) with the SESANS to see if we retrieve any useful data. This way we can measure porosity in the concrete and discuss if any follow up experiments can be planned to investigate more of these interactions.
Another proposed technique to measure the concrete is Scanning Electron Microscopy (SEM). This technique produces images of a sample by scanning it with a focused beam of electrons. Various signals are produced when the electrons interact with the atoms in the sample, which contain information about the sample's surface topography and composition. The resolution of SEM can be better than 1 nanometer. The idea is that the results of both of these techniques can be compared to draw any sensible conclusions about the materials.

2

Spin Echo Small Angle Neutron Scattering

2.1. SESANS

To understand the Spin-Echo Small Angle Neutron Scattering (SESANS) technique, a small introduction into the underlying processes is given below. The setup consists mainly of a polarized neutron in magnetic fields. How the polarized neutrons behave is crucial for the SESANS technique and will be explained in detail [5]. A polarized neutron has two eigenstates (due to the spin-vector), or if we look at a neutron as a wave instead of a particle: the neutron wave function is a superposition of two opposite eigenstates. The two eigenstates are parallel or anti-parallel to the magnetic field. The difference between the two states become visible in the magnetic field due to the different alignment of the states. The state anti-parallel to the magnetic field experiences a loss in potential energy, while the other state (parallel) experiences a gain in potential energy. This leads automatically to either a gain and a loss, respectively, because of the conservation of energy. This results in a deflection away or a a deflection towards the normal in the magnetic field. The neutrons with different eigenstates are parallel again after they have left the magnetic field, but there is clearly a separation visible. The distance between these two states is called the spin-echo-length z, which can be described as follows:

$$z = \frac{c\lambda^2 LB \tan(\theta_0)}{2\pi} \tag{2.1}$$

In this equation λ is the neutron wavelength, L is the length of the straight path in the magnetic field, B is the strength of the magnetic field and θ_0 is the angle of the foil and the incoming neutron. The easiest way to change the spin-echo-length is to change the magnetic field, because all the other parameters are usually not variable.

The SESANS setup is symmetric, which means that in the middle of the setup the directions of the magnetic fields reverse, which result in a spin-echo-situation. This is represented in Figure 2.1. Without a sample in the center of the setup, a beam gets refocused by the second magnetic field which brings the two different states back together. They then have exactly the same phase and so the original polarization is obtained. However, when a sample is placed in between the two opposite magnetic fields, scattering occurs. A small spin-echo-length z causes the two states of neutrons to be very close to each other. This way the states each experience the same scattering, because the sample usually has the same contents and characteristics on such a small scale. The phase states is medium dependent, so both functions have the same phase changes at the focusing point at the end of the setup, which results in the original spin orientation. This happens only as long both states scatter through the same density, because of the medium dependency. Something different happens, when the eigenstates take a different path through the sample with different media. This will result into a phase change and therefore a phase difference at the refocusing point. A depolarization can be measured in this way, because this leads to a different final spin orientation. The degree of depolarization saturates, when the spin-echo-length z is longer than the characteristic lengths inside the sample. The depolarization

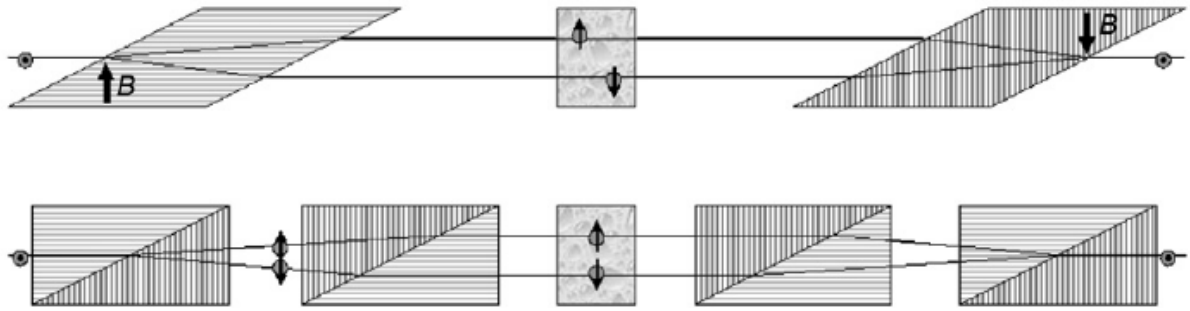

Figure 2.1: Schematic view of magnetic fields in SESANS

can be shown as follows:

$$\Sigma_t = \lambda^2 t(\Delta\rho_0)^2\varphi(1-\varphi)\xi \tag{2.2}$$

In this equation t is the thickness of the sample, $\Delta\rho_0$ is the neutron scattering length density, φ is the packing fraction and ξ is the correlation length of the sample inhomogeneities. The nm-μm range of material structures is investigated with SESANS. The SESANS approaches it as follows. The polarization P(z) of the neutron to the projection G(z) of the auto-correlation function γ(r) of the density distribution ρ(r) of the sample. The polarization P(z) is measured as a function of the spin-echo length. There is no need for collimation of the neutron, because the depolarization is only dependent on the phase difference between the two eigenstates. This is a major advantage in comparison with SANS. Multiple scattering effects are easily accounted for, so also thicker samples can be measured. In comparison with earlier techniques, the amount of scattering had to be reduced. The link between depolarization and size of sample inhomogeneities is used with the SESANS technique, as described above. The density distribution function describes the characteristics of the sample:

$$\rho(r) = \begin{cases} 1 & \text{if r is inside phase} \\ 0 & \text{otherwise} \end{cases} \tag{2.3}$$

The auto-correlation function can be constructed from the density distribution:

$$\gamma(r) = \frac{\int_V \Delta\rho(r')\Delta\rho(r'+r)dr'}{\int_V \Delta\rho(r')\Delta\rho(r')dr'} \tag{2.4}$$

The projection of this auto-correlation function of the density distribution can be deducted from the measured polarisation. The projection of the auto-correlation function G(z) can be obtained by performing an Abel transformation. For a spherically symmetric density distribution this projection is given by:

$$G(z) = \frac{2}{\xi}\int_z^\infty \frac{\gamma(r)r}{(r^2-z^2)^(1/2)}dr \tag{2.5}$$

with for the correlation length ξ:

$$\xi = 2\int_0^\infty \gamma(r)dr \tag{2.6}$$

The polarization P(z) comes out as raw data out of a measurement. The projection of the auto-correlation function of the density distribution is related to the polarisation as following:

$$P(z) = e^{\Sigma_t(G(z)-1)} \tag{2.7}$$

The condition on the right side of equation 2.6 is true for a SESANS device in the ideal case. The neutron, which does not go through the sample, has zero depolarization in this case. In practice this is usually not the case, therefore the polarization needs to be normalized with respect to the polarization of an empty neutron measurement. If there are no more sample inhomogeneities characteristics within the spin-echo length z, the polarization saturates. This means that the density distribution function is

zero. The final polarization, or the fractions of neutrons that does not scatter when traversing through the sample, can be written as:

$$P(\infty) = e_t^{\Sigma} \tag{2.8}$$

The auto-correlation of the density distribution can be obtained from the polarization:

$$G(z) = 1 - \frac{ln((P(z))}{ln(P(\infty))} \tag{2.9}$$

The outcome of a SESANS measurement [6] is visually analysed with use of the Figure 2.2 The height of the final polarization can be deducted from Equation 2.7. Another output that will show up quite clear in the graph is the maximum spin-echo length for when the density relations can still be seen in the sample: l_{max}. This is not the same as the ξ, correlation length as discussed earlier. The correlation length is the average length of all lines within the specific inhomogeneity of a sample.

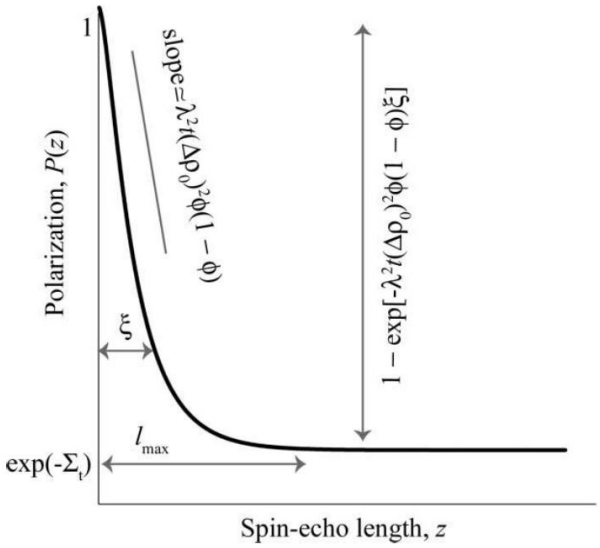

Figure 2.2: Interpretation of data in SESANS

The SESANS technique is used for this measurement, because it fits the scale to be investigated.

2.2. Fractal Geometry

The concept used to analyze the SESANS measurement is fractal geometry [7]. This concept provides a basis for describing materials whose structures are random or chaotic and yet possess scale invariance. Fractal functions are a good choice for modeling 3-D natural surface shapes because many physical processes produce a fractal surface shape and fractals are widely used as a graphics tool for generating natural-looking shapes. A few examples of materials which have this structure are branched clusters of colloidal silica particles formed by aggregation and submicroscopic pores in coals [8]. Studies of this system have revealed non-integral power-law density correlation functions. The defining characteristic of a fractal is that it has a fractional dimension, from which we get the word ”fractal”. Technically, a fractal is defined as a set for which the Hausdorff-Besiovich dimension is strictly larger than the topological dimension, i.e. a set for which the only consistent description of its metric properties requires a ”dimension” value larger than our standard, intuitive defenition of the set’s ”dimension”. In the case of the concrete we are looking at fractal surfaces (pores or particles) with a surface fractal dimension D_s or mass fractals with mass fractal dimension D_m. It is expected that for a surface fractal [6]:

$$I(Q) \propto Q^{-(6-D_s)} \tag{2.10}$$

and for a mass fractal:

$$I(Q) \propto Q^{-D_m} \tag{2.11}$$

where the values of both D_m and D_s are smaller than 3, the dimensionality of the Euclidian space. These proportionality's are for SANS measurements. For SANS the intensity of the scattered beam I(Q) can be factorized as follows:

$$I(Q) = \mathcal{B}P(Q)S(Q) \tag{2.12}$$

Here $\mathcal{B}$ is a pre-factor given by the neutron scattering length density contrast. P(Q) is the form factor characterizing the morphology/shape of the pores, and S(Q) is the structure factor corresponding to the correlations between the pores.

$$\mathcal{B} = \phi_D \Delta\rho^2 V_p = \phi_D \Delta\rho^2 4\pi l/3 \tag{2.13}$$

Here $\Delta\rho^2$ is the scattering length density contrast, V_p is the volume of a primary pore building block and l is the associated length.

$$\mathcal{P}(Q) = (1 + Q^2 l^2)^{(\mathcal{D}_s - 6)/2} \tag{2.14}$$

$$\mathcal{S}(Q) = 1 + \frac{\mathcal{D}_m \Gamma(\mathcal{D}_m - 1}{(2Ql)^{\mathcal{D}m}} (1 + \frac{1}{(Q\xi)^2})^{(1-\mathcal{D}_m)/2} \times \sin[(\mathcal{D}_m - 1)\arctan(Q\xi)] \tag{2.15}$$

To apply these fractal geometries to SESANS, first the Hankel transform has to be applied. Then these models can be used to fit the SESANS data and find the values for these coefficients. The Hankel transformation of the SANS cross section is given by:

$$\mathcal{G}'(z) = \int_0^\infty \mathcal{J}_0(Qz)\mathcal{I}(Q)QdQ \tag{2.16}$$

In which $\mathcal{J}_0$ is a zeroth-order Bessel function of the first kind. The idea is to fit the results of the SESANS to these functions in order to extract as much useful data.

2.3. Infinitely long Cylinder with diameter D

Another model to used to analyze the curves of SESANS is the model for infinitely long cylinders with diameter D [9]. In this model, the pores are seen as cylinders in the material. The following function for the polarization is observerd:

$$\mathcal{P}(z) = e^{\mathcal{G}(z) - \mathcal{G}(0)} \tag{2.17}$$

The correlation function $\gamma(r)$ for a right and infinitely long cylinder with a diameter D is:

$$\gamma(r) = \begin{cases} 1 - \mathcal{F}_1(1/2, 3/2; 3, \frac{r^2}{\mathcal{D}^2}) r^3 4\mathcal{D}^3 - \frac{\mathcal{F}_1(-1/2,3/2;2;r^2\mathcal{D}^2)r}{\mathcal{D}}, & 0 < D \\ 1 - \mathcal{F}_1(1/2, 3/2; 3; \frac{\mathcal{D}^2}{r^2}) \mathcal{D}^2 4r^2 - \mathcal{F}_1(-1/2, 3/2; 2; \mathcal{D}^2 r^2) & D < r < \infty \end{cases} \tag{2.18}$$

In this equation $\mathcal{F}_1$ is the Hypergeometric function. The projection G(z) is not possible to solve analytically, so a numerical solution is given in the following image. The $\gamma(r)$ and G(z) show a levelling decay saturating around D on the horizontal axis. To extract G(z) numerically equation 2.5 and 2.6 are used. Then P(z) is extracted from equation 2.16. This model can then fit the SESANS data with help of Matlab.

3

Scanning Electron Microscopy and X-ray Powder Diffraction

3.1. SEM

The Scanning Electron Microscope (SEM) is a type of electron microscope that produces images of a sample by scanning it with a focused beam of electrons. An electron beam is focused on the sample and there the electrons interact with the atoms in the sample [10]. This interaction produces various signals that contain information about the sample's surface topography and composition. The measurements were performed at Delft Aerospace Structures and Materials Laboratory can achieve a resolution up to 3.5 nanometer and the sample can be observed in a wide range of conditions, from changing temperature to humidity.
Usually the detection of secondary electrons emitted excited by the electron beam is the most common technique to obtain pictures of the sample's surface. By scanning the sample and collecting the secondary electrons that are emitted using a special detector, an image displaying the topography of the surface is created. The used SEM is configured with both secondary and back-scattered electron detectors as well as an energy dispersive X-ray spectrometer.

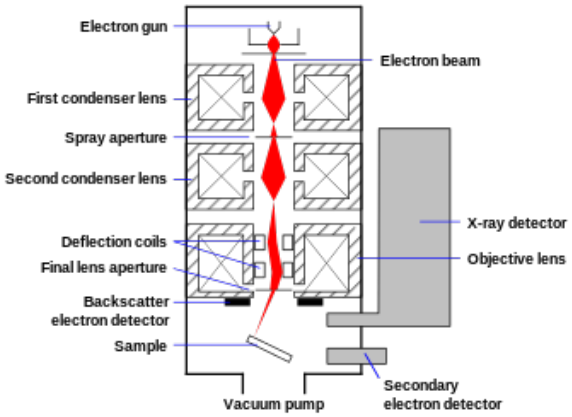

Figure 3.1: Schematic view a Scanning Electron Microscope (SEM)

A typical SEM begins with an electron beam, which is emitted from an electron gun [11]. Normally it is a tungsten filament cathode which is put on high voltage for electrons to escape the cathode. This electron beam has an energy range of 5 keV to 35 keV and is focused by one or two condenser lenses to a spot about 0.4 to 5 nm in diameter. To scan the whole sample, the beam passes a pair of scanning coils or deflector plates in the electron column. This can deflect the beam in the x and y direction, so it can scan the whole surface of the sample.
When the electrons interact with the sample, they lose energy by repeated random scattering and

absorption in the sample. The volume in which this can happen for the electrons is called the interaction volume, with a minimum of around 100 nm to a maximum of approximately 5 micrometers. The interaction volume depends on the sample's density, the electron's energy and the atomic number of the sample. This results in reflected high-energy electrons by elastic scattering and in emission of secondary electrons by inelastic scattering.
The magnification in the SEM used is in the orders of magnitude from about 20 to 300,000 times. The magnification results from the ratio of the dimensions of the raster on the sample and the raster on the display device. In most of the SEMs the display screen has a fixed size, so higher magnification results from reducing the size of the raster on the sample. It is therefore controlled by the current supplied to the x and y scanning coils, or the the voltage supplied to the x y deflector plates.
The Everhart-Thornley detector is the detector for the low-energy (<50 eV) secondary electrons that are ejected from the k-shell of the sample's atoms by inelastic scattering interactions with beam electrons. These electrons originate within a few nanometers from the sample surface, due to their low energy. These electrons are first collected with a biased grid at about +400 V and then further accelerated towards a phosphor or scintillator positively biased to about +2,000 V. Now the secondary electrons are sufficiently energetic to case the scintillator to emit flashes of light, which are conducted to a photomultiplier outside the SEM column via a light pipe and a window in the wall of the sample chamber. This amplified electrical signal output by the photomultiplier is displayed as a two-dimensional intensity distribution that can be viewed and photographed and saved as a digital image.
The brightness of the signal depends on the number of secondary electrons reaching the detector. The activated region is uniform about the axis of the beam, if the beam enters the sample perpendicular to the surface. A certain number of electrons escape from within the sample. As the angle of incidence increases, the escape distance of one side of the beam decreases and so more secondary electrons will be emitted. This results in brightness for more steep surfaces and edges than flat surfaces, in which a well-defined image appears in 3D.
Two samples were measured with SEM. A CEMI and a CEMIII sample were measured without chemical degradation. First the samples are coated with a layer of gold with a thickness of a few nanometers, using a sputter coater. A Quorum 300 (Q300) was used to do this. Sputter coating is the standard method for preparing non-conducting or poorly conducting specimens prior to observation in a scanning electron microscope (SEM). After the coating process, the samples were examined one by one with the

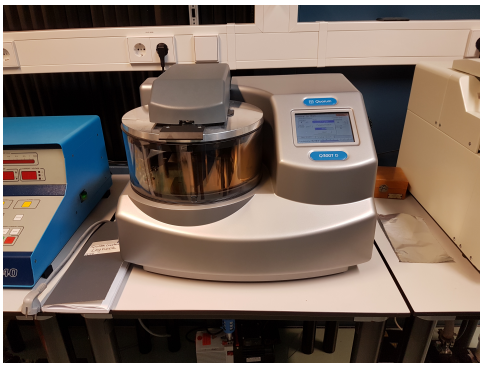

Figure 3.2: Sputter Coater: Quorum 300

SEM. At different magnification levels pictures were taken to obtain a better quality of the image and a deeper insight of the sample. At these same spots the EDX was performed to give an insight of the chemical composition of the concrete.

3.2. Energy-dispersive X-ray spectroscopy (EDX)

Apart from the surface structure, other signals can also be measured using specialized detectors. One of them is EDX, which can measure the element composition of a certain area. X-rays are generated within the whole of the interaction volume and the typical spatial resolution for X-ray micro-analysis in the SEM is of the order of a few microns.
There are two types of X-rays produced in the interaction between the electron beam and the sample, namely the Bremsstrahlung (translated: braking radiation) and the Characteristic X-rays. The

Bremsstrahlung X-rays are produced by slowing down of the primary beam electrons by the electric field surrounding the nuclei of the atoms in the sample. It is also known as continuum of background X-rays. The X-ray spectrum has an upper limit known as the Duane-Hunt limit, because the X-rays cannot have a bigger energy than the electron energy of the primary beam. The primary beam electron can lose all its energy in a single interaction event, in which the X-ray will have an energy equal to the electron $\mathcal{E}_0$. Usually the energy is lost in a number of interactions. A lot of X-rays are generated at low energy. However, the detector is not sensitive at low energy, so a 'whale' is observed for these X-rays. Atoms of each element in the sample consists of a nucleus made up of neutrons and positively charged protons, and a cloud of negatively charged electrons that surround the nucleus. Z is the number of protons in the nucleus of the atom, which defines the atomic number. Off course in a neutrally charged atom, the number of protons is matched with the number of electrons. The electron cloud is ordered in so-called electron shells. The shell closest to the nucleus is called the K shell, followed by L, M, N, O, P and Q shells. For EDX the K, L, and M shells are the most important. The number of electrons in each shell is obtained from quantum mechanics. K has a maximum of two electrons; eight for the L shell; 18 for the M shell and so on. Each shell, apart from the K shell, also has their own sub-shells.
The electrons with the highest ionization energy are in the K shell in the atom. This means more energy is needed to remove an electron from this shell further from the nucleus. Due to the attractive force of the nucleus, the further from the nucleus the electron is, the lower its ionization energy is. Characteristic X-rays are produced by electron transitions between the electron shells and sub-shells. An electron is removed from one of the inner shells of the atom by an electron from the primary beam so that the atom is ionized and in an unstable state. Then the atom regains stability when an electron from an outer shell fills the inner shell vacancy and an X-ray photon is emitted. Its energy is exactly the equal to the difference between the ionization energies of the electrons involved in the transition. Each element has its own specific ionization energies for each sub-shell, so the difference between the energies is characteristic of the element involved in producing the X-ray photon. In spectroscopy the most commonly used naming convention for Characteristic X-ray lines is the Sieghbahn notation. First the element is named as first component. Second the electron shell that was ionized to produce the X-ray, e.g. K, L, M, is named. Third the relative intensity of the line within each shell, e.g. α is the most intense line, followed by β and γ.
The EDX spectrum is the addition of the Bremsstrahlung X-ray spectrum with the Characteristic X-ray spectrum. The height of the X-ray peaks in an ED spectrum is given in X-ray counts (or counts per second). The concentration of the elements influences the peak height in the ED spectrum. The number of electrons in the primary electron beam is directly proportional to the number of X-rays generated from the sample and the number of X-ray counts recorded in the X-ray spectrum. If the beam current is increased, the number of X-rays is increased but this will not change the relative heights of the Characteristic X-ray peaks in the spectrum. It is important that the accelerating voltage is high enough to overcome the ionization energy of the elements in the sample. Otherwise no X-rays will be generated by some elements and wrong results are obtained for the composition. To know if there is enough accelerating voltage, the overvoltage ratio is calculated by the following equation:

$$\mathcal{U} = \frac{\mathcal{E}_0}{\mathcal{E}_c} \tag{3.1}$$

In which E_c. This ratio has to be at least 2 (the optimum value is ≈2.7), for efficient generation of X-rays.

3.3. X-ray Powder Diffraction

Besides the SEM and EDS measurements, also another technique is used. It is called X-ray Powder Diffraction (XRD) and these were executed at the Reactor Institute. This is a rapid analytical technique primarily used for phase identification of a crystalline material. Primarily, only powders are used with this machine, but solids can also be investigated. For material science this is a perfect way to analyse crystalline constitutions of material samples. It reveals structural information, such as chemical composition, crystal structure, crystallite size, strain, preferred orientation and layer thickness.
At the RID the PANalytical X'Pert Pro is used, which uses a rotating x-ray canon and a detector to analyze the X-rays. This type of diffractometer is primarily used to identify individual minerals and mineral mixtures (rocks). The sample is placed in a holder, which is perfectly aligned to obtain the

correct angle with the diffractometer. An X-ray diffraction pattern is a plot of the intensity of X-rays scattered at different angles by a sample [12]. It is important that the sample's surface is smooth for the measurement with XRD. The voltage and current of the x-rays was set at 45 kV and 40 mA, respectively. In this machine the intensity for different angles of 2θ is measured. The intensity is measured

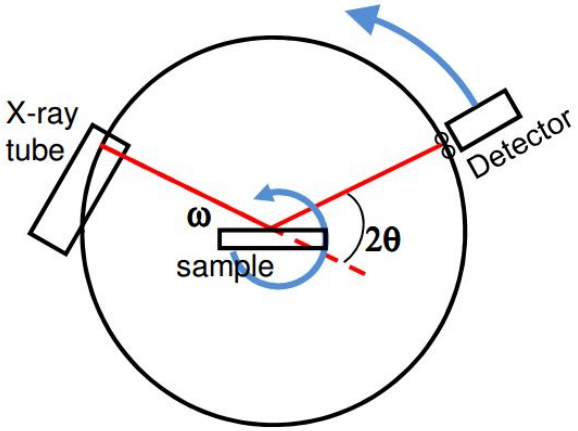

Figure 3.3: Schematic view a X-ray Powder Diffraction (XRD)

as relative counts or 'arbitrary units'. This results into a diffractogram beginning from 5 degrees until 80 degrees with their arbitrary units in intensity, which shows the relative intensity peaks.
With use of the software FullProf the data can be analyzed to match the intensity peaks with various minerals and salts. This can be very time consuming, but if there is already an idea of what possible compounds might be present, this makes the process easier. Each "phase" produces a unique diffraction pattern.
A phase is a specific chemistry and atomic arrangement. Quartz, cristobalite, and glass are all different phases of SiO_2. They are chemically identical, but the atoms are arranged differently. Amorphous materials, like glass, do not produce sharp diffraction peaks. The example of SiO_2 is given below how the final diffractogram would look like.

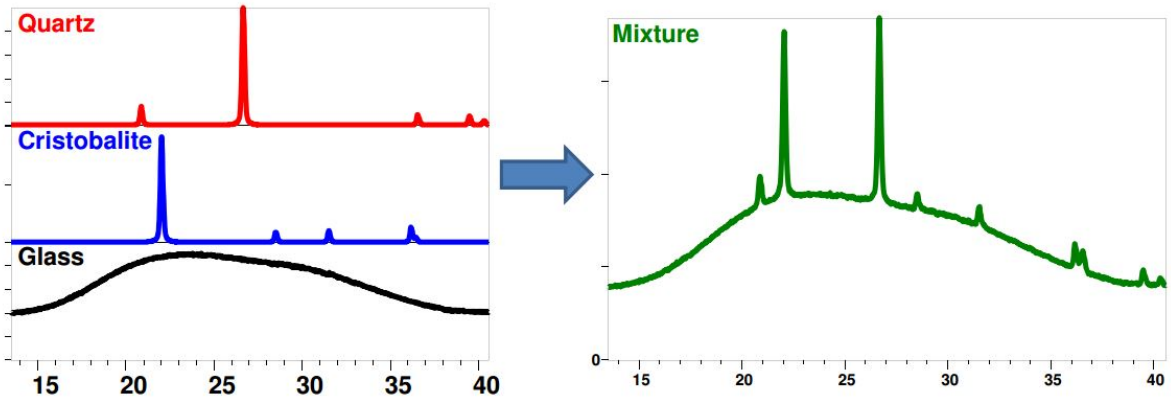

Figure 3.4: Example of XRD

4

Overview of Geological Repository

Portland cement is exceptionally durable and therefore the world's most widely used construction material as well for the geological repositories. However, material limitations, design and construction practices, and severe exposure conditions can cause concrete to deteriorate, which may result in functional or structural problems. In this research we are looking at three forms of deterioration, which are most likely to occur at the contact interface between the host rock Boom Clay and the concrete geological repository[3]. Chemical corrosion is one of the most significant elements which effects the durability of concrete. This is because of the solubility and alkalinity of calcium hydrate in concrete, as well as the porosity of concrete. These forms are the effects of chloride attack, carbonation and sulfate attack. Every part of the geological repository has their own recipe for cementitious materials to fulfill all their requirements. In this research two types of concrete are investigated and here is explained what they are used for in the repository.

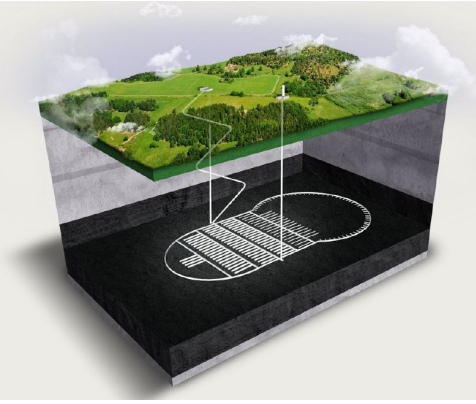

Figure 4.1: The proposed repository by OPERA

4.1. Cementitious Materials

In this research two types of concrete are investigated, namely CEM I SR 3 and CEM III/B 42.5 LH/SR. From now on these types of concrete are called CEM I and CEM III. CEM I is Portland cement without any main addition and CEM III is Blastfurnace cement, in which the main addition is sand. There are different recipes for the different purposes in the geological repository provided by COVRA. Two concretes are investigated, namely the foamed concrete for the backfill and the concrete for the conditioning (of 200 l LILW drums). The function of the backfill is to enclose the emplaced waste during the operational phase of the geological repository. In a so-called 'fail-safe situation', the enclosure should prevent the waste packages coming into contact with water in the unlikely case of flooding of the facility. As a consequence, the hardening time, the fluid properties and hardened properties of the cementitious material of the enclosure are relevant [1]. The goal of conditioning nuclear waste

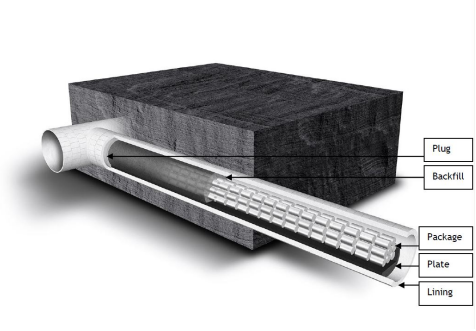

Figure 4.2: One gallery of the proposed repository by OPERA

is to convert radioactive waste materials into a form that is suitable for its subsequent management, such as transportation, storage and final disposal. Conditioning processes can also come in the form of vitrification, but we are looking off course at cementation. The type of waste makes this cement a good option for conditioning. In general the solid wastes are placed into containers. The grout is then added into this container and allowed to set. The container with the now monolithic block of concrete/waste is then suitable for storage and disposal.

4.1.1. Backfill concrete

Foamed concrete consists of cement, water, foam and (fine) aggregates. Given the demands of the project, normally first the density(limit) is chosen [3][1]. The density of the foam concrete is smaller than 2300 kg/m^3. A desired strength is chosen, depending on the specific constraints. Based on this strength, the amount of water, foam and in some cases, aggregates are calculated. Following is the used recipe for the enclosure emplaced waste (backfill - foam concrete) used for the experiments.

Table 4.1: Recipe for foamed concrete with CEM I

Component	Receipt for 1 m^3 of Aercrete FC 1200 to 1600 kg m^{-3}	Type for OPERA	1200 kg m^{-3}	1600 kg m^{-3}	
Cement	360 to 400 kg	CEM I SR 3 <3% C_3A	360	400	kg m^{-3}
Water	140 to 160 kg	-	140	160	kg m^{-3}
Fine aggregate	750 to 1100 kg	Quartz sand: 0-4 mm	750	1100	kg m^{-3}
Foaming agent Synthetic surfactant	0.57 to 0.36 l	Foaming agent TM 80/23 Synthetic	1	1	kg m^{-3}
Water	21.3 to 13.6 l	Water	21.3	13.6	kg m^{-3}
Air	434 to 277 l	Air	0	0	kg m^{-3}

It has a minimum compressive strength of 10 MPa (in case of drying 28 days). The dry density is from 1200 until 1600 kg/m^3. The foaming agents can be combined with CEM I or CEM III, but not with fly ash. There is a preference for CEM I (Portland cement) and CEM III because a larger lifetime of the steel envelopes is expected with the use of CEM I. This backfill needs to fulfill certain requirements for its purpose. The density of the mortar needs to be smaller than the emplaced waste packages to prevent floating of these packages during the operational phase. It is expected to be smaller than 2300 kg/m^3. The concrete is is actually a suspension and must not show relevant segregation and/or bleeding. Bleeding is a form of segregation where some of the water in the concrete tends to rise to the surface of the freshly placed material. This arises due to the inability of the solid components of the concrete to hold all of the mixing water when they settle downwards (water being the lightest of all the mix constituents). Bleeding of the water continues until the cement paste has stiffened enough to end the sedimentation process. To do this in the proposed repository of OPERA, a minimum volume of 322 m^3 is to be backfilled. To prevent segregation or bleeding and to organize a successive emplacement of waste, this has to be done in one (working day). The concrete should be strong enough to hold pressure and should prevent the cave-in of the supercontainer, when the concrete segements in the lining no longer provide mechanical support. A high pH of the backfill is useful for the durability of the

steel envelope of the supercontainer (containing HLW) and steel containers (containing LILW). There is also a thermal conductivity constraint on the backfill, because heat generating waste is also contained in the repository. The backfill shouldn't act as a thermal insulator, so a minimum value in thermal conductivity of 1 $Wm^{-1}K^{-1}$ is sufficient. Next it should adapt for the unlikely case of flooding. The concrete should prevent leaching of radionuclides from the waste package. There should also be no degradation by seawater for one year. The backfill should actually be impermeable [13].

4.1.2. Conditioning concrete

Another type of concrete is also investigated. This concrete is used for conditioning and is made with blast furnace slag cement, water, aggregates and plasticisers. The recipe is shown below. It is used for the LILW waste drum. Most of the volume of LILW collected by COVRA is solid, compactable waste. Its volume is reduced by compacting the waste-containing drums with a 1,500-tonne super compactor. The compacted drums (pucks) are then transferred to drums with a larger diameter and conditioned with concrete. The super compactor has been in operation since 1992.

Table 4.2: Concrete composition for the disposal of compacted waste in 200-litre drums

Component	Receipt for 1 m^3 of Aercrete FC 1200 to 1600 kg m^{-3}	Type for OPERA	1200 kg m^{-3}	1600 kg m^{-3}	
Cement	360 to 400 kg	CEM III/B 42.5 LH/SR	360	400	kg m^{-3}
Water	140 to 160 kg	-	140	160	kg m^{-3}
Fine aggregate	750 to 1100 kg	Quartz sand: 0-4 mm	750	1100	kg m^{-3}
Foaming agent Synthetic surfactant	0.57 to 0.36 l	Foaming agent TM 80/23 Synthetic	1	1	kg m^{-3}
Water	21.3 to 13.6 l	Water	21.3	13.6	kg m^{-3}
Air	434 to 277 l	Air	0	0	kg m^{-3}

The 200 liter drums its measurements and contents is shown in the following image[3].

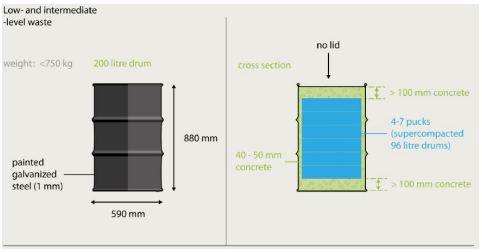

Figure 4.3: 200 liter drums

5

Experiments

5.1. Sample Preparation

In this research concrete degraded by three different processes: carbonation, chloride attack and sulphate ingress is investigated. In order to do measurements with the concrete, samples have to be prepared first. This is done by cutting the samples and degrading them in certain solutions.

5.1.1. Cutting the Concrete Samples

The concrete samples are provided by COVRA. It is cylindrical form with a radius of 3 cm and a length of 5 cm. The concrete was casted in May 2016. The samples are prepared at the Microlab of the TU Delft. It is situated in the faculty of Civil Engineering & Geosciences. The goal is to cut samples of the same radius as the cylinder, but with a thickness of 1 mm. This is the required thickness for samples being investigated with SESANS. First the cylinder is polished on one side using a "grinder", because the samples have to be smooth on both sides. Then a glass plate is glued to the polished side. It is important for the other side of the glass plate to be clean, because it will be stuck to a vacuum pump. The glass plate along with the concrete is placed into the "sawing machine". This machine has a diamond rotor blade, so is able to cut through concrete. To saw a smooth cut through the concrete, the glass plate is held using a vacuum pump. Water is pumped to the blade to prevent the blade from overheating. The cylinder is cut half way, then the sample is flipped to cut all the way through. This is for safety, otherwise your fingers would come to close to the rotor blade. The end product is a concrete sample of around two mm thick on a glass plate (this is the smallest thickness, which can be cut, otherwise the concrete could break).
The next step is to get the two mm concrete sample to the desired one mm. This is done using a rough polisher. The concrete sample on the glass plate is attached to a 'mouse' using a small mechanical vacuum pump. The mouse has four screws at each corner, which have to be turned just out of the mouse. This mouse is placed on a deck with 1000 µm plates to obtain the right measurements for the samples. Then the screws are again turned into the mouse, so the distance between the glass plate and the polisher is almost exactly 1 mm. It is important that all the four screws are turned right, otherwise the sample will be polished skew. The mouse with the sample is put on the polisher and polished until there is no more noise. This means there is no concrete left to be polished, so the sample is 1 mm. At the end we succeeded to manufacture 10 of these samples, which are all almost exactly 1 mm.

5.1.2. Degradation of the Concrete Samples

The samples will be chemically degraded to mimic the conditions at the environment of the geological repository, which is quite similar to sea water at large depth. The main source of $CO_2(g)$ is the atmosphere. It is generally stated that the partial pressure of $CO_2(g)$ in the atmosphere is 10-3.5 atm, which corresponds with 316 ppm (or 32 Pa). Another important source of carbon dioxide is (micro)biological activity in soil systems (soil carbon cycle). The solutions used are examples of what is existent at that depth in the water. This might not be the correct salts to use, but these solutions were also used in literature, so this makes it easier to draw conclusions [14]. The samples will be prepared in three ways:

Samples will be put in a tank with high concentration of CO_2. This is a way to investigate the carbonation of the concrete. Carbonation is a process of CO_2 diffusion into the specimen. This results into a reaction of carbon dioxide with calcium hydroxide in concrete to form calcium carbonate, which is chemically described as:

$$Ca(OH)_2 + CO_2 \rightarrow CaCO_3 + H_2O \tag{5.1}$$

This is a very slow and continuous process, which slows down with increasing diffusion depth. This reaction increases mechanical strength of concrete. However it decreases the alkalinity, which is essential for corrosion prevention of the reinforcement steel. It is thus an unwanted process for concrete used in the geological repository [14]. It is interesting to look at these effects, because the CO_2 level underground is much higher than the earth's surface.
Samples will be degraded with use of sulfates. In this research Na_2SO_4 is used.Sulphate attack is the geochemical process in which dissolved sulphate species reacts with cement components with the precipitation of sulphate minerals as gypsum, ettringite and thaumasite. The sources of sulfates are from the underground water and from pyrite oxidation. Pyrite is always present in marine environments. The oxidation of pyrite results in the production of protons (acidification) and sulphate ions, both of which may participate in detrimental reactions affecting concrete durability. The investigated process is external sulphate attack, which leads to formation of Gypsum $CaSO_4 \cdot 2\,H_2O$, ettringite $Ca_6Al_2(SO_4)_3(OH)_{12} \cdot 26\,H_2O$ and thaumasite $Ca_3Si(OH)_6(CO_3)(SO_4) \cdot 12\,H_2O$. Ettringite is formed in hydrated ordinary Portland cement (CEMI) as a result of calcium aluminate and calcium sulfate:

$$C_3A + 2\,CaSO_4 \rightarrow \text{ettringite} \tag{5.2}$$

Here the C is CaO and A is Al_2O_3, which is a commonly used in chemistry for concrete.
During the construction phase, sulphate attack (originating from both pyrite oxidation and the native Boom Clay water) on concrete liners remain an important concern. Sulfates in solution in contact with concrete can cause chemical changes to the cement. The sulfate will corrode the concrete, because of its alkalinity. This is called corrosion. This causes significant micro-structural effects leading to the weakening of the cement binder. It can also cause damage to porous cementitious materials through crystallization and recrystallization. It is interesting to look at this form of degradation, because sulfates are present in many forms in nature. This dissociation reaction is chemically described as:

$$Na_2SO_4 \rightarrow 2\,Na^+ + {SO_4}^{2-} \tag{5.3}$$

Samples will be degraded with use of chloride attack. Reinforced concrete exposed to chloride ions is the primary cause of premature corrosion of steel enforcement. It can cause steel corrosion if oxygen and moisture are also available to sustain the reaction [15]. Chlorides dissolved in water can permeate through sound concrete or reach steel through cracks. Chloride containing admixtures can also cause corrosion. The risk of corrosion increases as the chloride content of concrete increases. If the threshold value (certain limit of chloride content at the surface of steel) is exceeded, corrosion will occur if water and oxygen are available.

$$NH_4Cl \rightarrow {NH_4}^+ + Cl^- \tag{5.4}$$

Two concrete samples (CEMI and CEMIII) were put in a carbonation chamber at the Civil Engineering Faculty. The chamber had a CO_2 percentage of 3% and a relative humidity of 75%. The time spent in the chamber was two weeks. This is also an environment likely to occur at the geological repository. The conditions are very humid and the CO_2 concentration is way higher than at the earth's surface, because of the hydrostatic pressure. The CO_2 partial pressure is around 10-2.4 atm. Next there were two samples chemically degraded. A CEMI sample was put in a Na_2SO_4 solution with a concentration of 33,8 g/L. A CEMIII sample was put in a NH_4Cl solution with a concentration of 9,8 g/L. The pH of these solutions were measured before the start of the degradation, which were pH=5.10 for the NH_4Cl and pH = 5.66 for the Na_2SO_4 solution. Also these samples were left for a degradation of two weeks. Samples without degradation were investigated as well in order to compare them with degraded samples and identify possible changes over time.

5.2. Chemistry

It is known from literature that chloride penetration and carbonation can occur simultaneously, but this could not be planned for measurements. Carbonation of concrete should decrease the porosity of the

Figure 5.1: Carbonation chamber

samples, because the pores get clocked by the calcite $CaCO_3$ precipitation. This way the penetration of the chloride ions (chloride attack) is decreased, because the diffusion process is obstructed [16].The actual carbonation rate depends on a number of other factors. The main ones are related to the fact that the CO_2 ingress in the cementitious material is a diffusion-controlled. process.
It is observed that carbonation slows down when water/cement ratios are lower, because total porosity (and capillary porosity) is lower for lower water/cement ratios[17]. It can either corrode the concrete or add strength to the structure due to the clocking of the pores. Ordinary Portland concrete (CEMI) is assumed to densify, because there are a lot of carbonates available to react with the carbon dioxide. This will reduce porosity and permeability of the concrete. The concentration of CO_2 and the temperature influences the carbonation process severely. At an humidity higher than 70 percent the process is slowed down, because the moisture in the pores slower the rate of diffusion. However, when the humidity is too low under 50 percent the process is slowed down, because the moisture level is insufficient [16]. The resistance of carbonation is a material property and can only be compensated by a higher concentration of CO_2.
From the initial pH of 5.1 an increase of pH was noticed after immersing the CEM I sample in the Na_2SO_4 solution after 2 days of stirring. Sodium and potassium have an effect on the $pHopera_3$. A decrease of pH over time was observed during the two weeks contact time for degradation.
Chloride attack also causes severe deterioration in concrete. Chloride ions are diffused through the pore network and micro-cracks of the concrete. Steel reinforcement are effected by the chlorides, which accelerate the deterioration.
Concrete is a heterogeneous material, which is composed by aggregates. The aggregates are hold together by a binding hardened cement paste. The porosity is dependent on the hydration level and could be in any geometry form.

6

Analysis of SESANS

6.1. Visual Interpretation

To analyse the raw data of SESANS roughly by eye is quite easy. Already mentioned in at image 2.2 in Section 2, the output graph is given here.

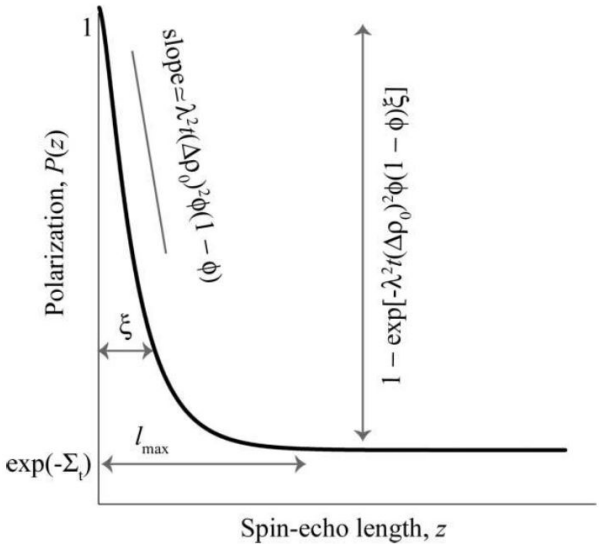

Figure 6.1: Interpretation of data in SESANS

This graph gives several sample characteristics.

- l_{max} The maximum sphin echo length l_{max} occurs at a point where the depolarization is satisfied. The final polarization is thus set when there are no more density relations in the sample. The sample is in a disk form, so the diameter D should be equal:

$$l_{max} = \mathcal{D} \tag{6.1}$$

  The final polarization should lay within the reach of SESANS, in order to be able to determine the diameter.

- ξ As already mentioned, for the correlation length of the spherical sample inhomogeneities is applicable:

$$\xi = \frac{3}{4\mathcal{D}} \tag{6.2}$$

- P(∞) The height of the final depolarisation is directly related to the diameter of the sample characteristics. The final polarisation level will decrease if the diameter increases.

- dP(z)/dz The inital slope of the curve is proportional to the chemical composition $\Delta\rho_0$ and the packing fraction ϕ of the sample characteristics, and almost independent of the arrangement of the inhomogeneities.

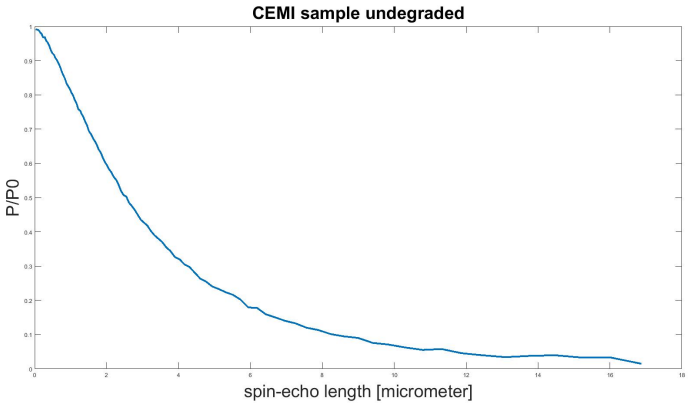

Figure 6.2: SESANS measurement of CEMI

The same sample was also measured after two weeks of carbonation, but no difference was analyzed. The carbonation is a slow process, so this indicates the samples needs to have a longer time in the carbonation chamber for the sample to change chemically.
The problem is that it is unknown when the depolarization is satisfied. This means that extracting data from the visual analysis are not reproducible and cannot be of value for any conclusions. Other models have to be for the analysis. The depolarization increases after degradation, but decreases severely

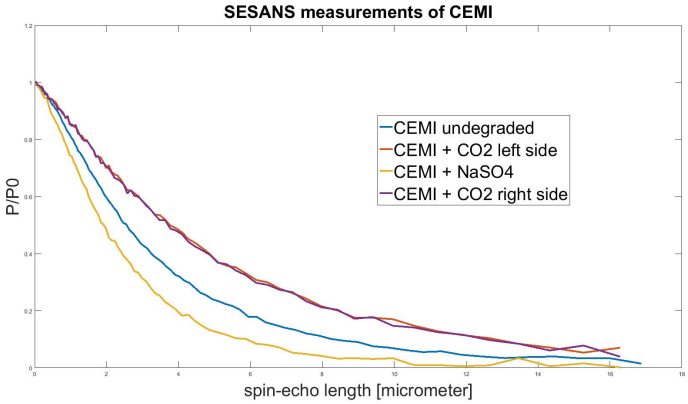

Figure 6.3: SESANS measurements of CEMI

after the degradation in the chemical solutions than the carbonation. The curves have nearly the same shape. First a strong decay in depolarization and then a longer decaying tail. This clearly indicates the anisotropic characteristic of the concrete in all the samples. The CEMI (with (CO_2)) sample was measured two times at different parts of the sample, because the sample looked like it had been carbonated only on one side. The outcome was that there was actually no difference at all, so even at sight the carbonation process is misleading. The measurements show that the chemical degradation clearly made some effect on the concrete samples. The samples are definitely more porous after the degradation due to the steeper slope of the depolarization. Besides it is more porous, the pores have also become bigger in the samples. What we know from our assumptions is that with higher contact time in the solution, the nano-pores will be clogged due to precipitation. This means there will be less depolarization in the curves, because the material will be more homogenous in forms of phase. The material becomes more solid because the pores, which are first filled by air or water, will be now solid. This is because the depolarization is due to the contrast between materials in phases (solid, gas

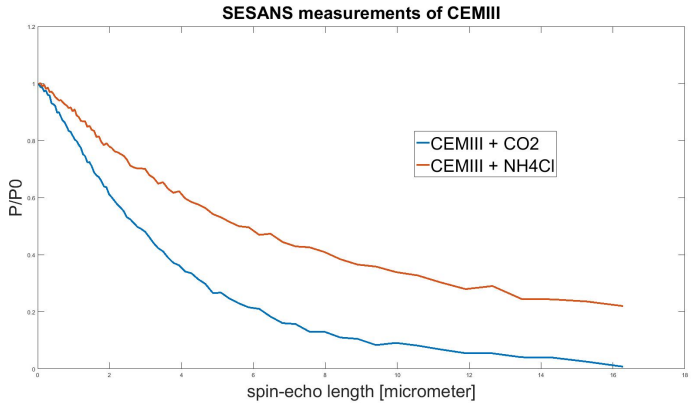

Figure 6.4: SESANS measurements of CEMIII

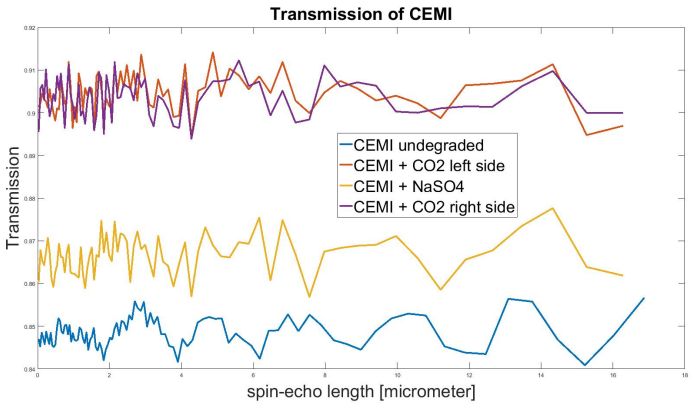

Figure 6.5: Transmission of CEMI samples

or liquid) and not the type of material. The curves are quite steep, because the pore sizes are very variable. This can predict that the material is poly-disperse. So clogging results in less scattering and more moisture in the pores results into more scattering.
For image 6.3 the CEMI samples are compared by SESANS. It is seen that carbonated CEMI sample has the highest depolarization. This is because the carbonation process causes precipitation inside the pores. The pores get clocked by the calcite. This way less neutrons are scattered, because the media of the sample is more homogeneous. The undegraded sample is thus more porous than the sample degraded by CO_2. Then the sample degraded by sulfate attack is severely affected. This sample has been softened and corroded in a harmful way. This means the pores have become bigger in the sample and no precipitation has appeared in the sample.
For image 6.4 the CEMIII samples have been measured by SESANS. It is clear that the same arguments can be used as in the CEMI samples. The carbonation causes precipitation in the pores, which causes the clocking. However, the chloride attack corrodes the concrete severely and enlarges the amount of pores. No precipitation is obtained, because of this chemical solution in contact with the sample. The undegraded CEMIII sample has unfortunately not been measured. We can estimate that this curve will lie in between the two other curves.
The transmission indicates the the amount of moisture in the sample. As seen in figure 6.5, the undegraded sample has the least amount of moisture content. The carbonated sample has the highest moisture content. This is logical, because this sample was kept in a tank with 70% relative humidity. The sample degraded by sulfate is in between the undegraded and the carbonated sample, with respect to moisture content. This is plausible this sample has been in solution for two weeks, but the pores have also been effected, so this sample cannot contain as much moisture. The pores are are damaged and the sample has been corroded overall, so this makes the amount of moisture to be hold also smaller.

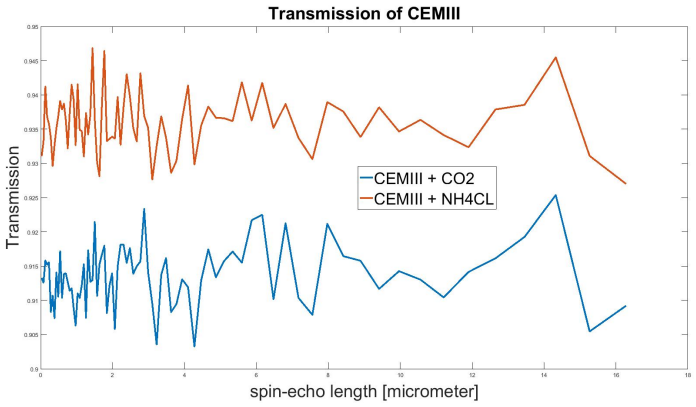

Figure 6.6: Transmission of CEMI samples

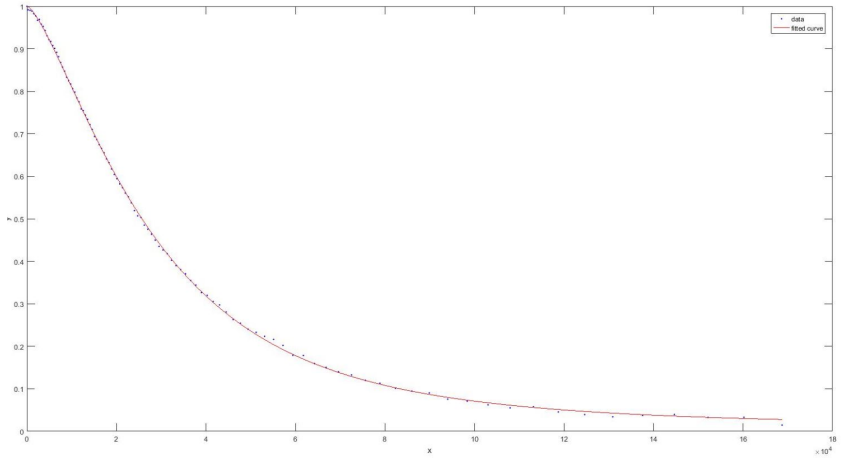

Figure 6.7: Test sample with surface fractal fit

The transmission for the CEMIII sample in figure 6.6 can also be explained by the same arguments as in the CEMI sample. The carbonated sample has a higher moisture content, because of the high humidity in the carbonation tank. The sample degraded by chloride attack contains less moisture, because of the affected porosity, which could contain the moisture.

6.2. Surface Fractal Model

With the trial sample we extracted a very nice fit with only the surface fractal model. All parameters weren't fixed and we extracted the following coefficients:

$$\mathcal{D}_s = 2.518$$
$$l = 7.941\mu m$$
$$sigma = 4.388$$

The surface fractal model was a very good fit to the test-sample of CEMI. That's why the surface fractal model was chosen to also fit the other four sample's results. The four samples were fitted with the surface fractal model. They were fitted correctly with use of Matlab and the following values for the coefficients were obtained: An explanation for the decreasing associated length scale L can be found in the following image. The length scale L gives the periodicity of the roughness of the sample. A relatively big associated length, results into a bigger roughness of the surface and vice versa. Thus with degradation the surface becomes smoother. This is quite obvious, because the surface is in direct contact with the degradation solution. Also the rough projections have the biggest surface contact with the solution, so these will be degraded the fastest. This way the smoothing of the surface happens

Table 6.1: Fitting values for the Surface Fractal Model

Fitting Values	CEMI + CO2	CEMIII + CO2	CEMI + NaSO4	CEMIII + NH4Cl
D_s	2.769	2.723	2.523	0.773
L (micrometer)	1.92	1.341	0.7951	1.034
sigma	5.585	5.691	6.174	1.98

very fast.

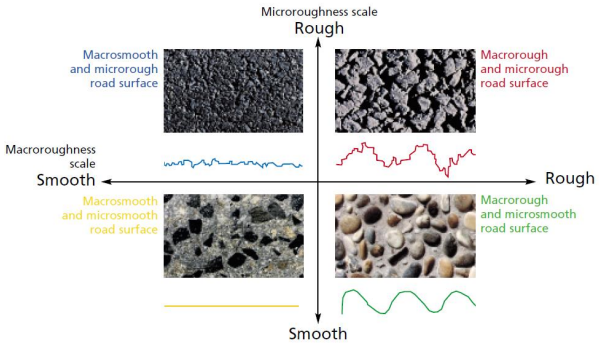

Figure 6.8: Associated length visualization

The explanation for the fractal dimension value $\mathcal{D}_s$ is hard to explain. It is correct that all the values are under 3, because this is obligatory in Euclidean space and for a surface fractal. The value decreases with degradation, which should be explained more thoroughly.

6.3. Infinitely long Cylinder with diameter D

[h] This model was computed with Matlab, but without any solid results. The script was constructed, but it was concluded that the computation time would be enormous to fit the data. Clusters of the TU Delft should be used to shorten this measurement time to a realistic limit. The reason for this was the numeric integrals should be calculated for very small steps of spin-echo length to obtain an accurate fit. There are also some other complications, such as the mathematics in 2.5. In this particular model r=z, which makes the numerator 0 in the bottom limit. This will make the script more difficult to compute, because different boundary conditions should be taken into account. Another difficulty is that the functions for theɣ(r) should be definite values, however the in the other equations to compute the G(z) and the ξ, integration will take place over r. This makes r both a constant in one case and a variable in the other equations. To compute this, way more complicated lines of code should be taken into account, which wasn't expected. The fact that the G(z) is not given, but has to be computed through Abel transformation (from ɣ(r) to G(z)) makes this model a project on itself.

7

Analysis of SEM, EDX and XRD

The following images were taken with the SEM. The surface structure is very porous, but also very different at different spots. It is a very chaotic sight and different kind of structures like crystals and the pores sizes vary from scales of nanometers to several micrometers. The pores in CEMI are in the orders of magnitude of tens of μm, but the smallest pore which was found was 0.38 μm. The CEM III has a higher porosity compared to CEM I specimens. This was analysed by counting the pores for the 50x magnification for both CEMI and CEMIII. Interesting was to see the micro-cracks in the CEMIII sample. The micro-structure of hydrated Portland cement pastes varies considerably with factors such as the chemistry and fineness of the cement used, the water: cement ratio, the use of chemical admixtures, variations in mixing procedures, differences in early curing temperatures, and variations in hydration conditions [18]. The images of the concrete depend on many different conditions, but an attempt has been made to describe the images as accurate as possible. The magnification of the SEM is stated in the black bar at the bottom of every image. At the magnification level of 50x the

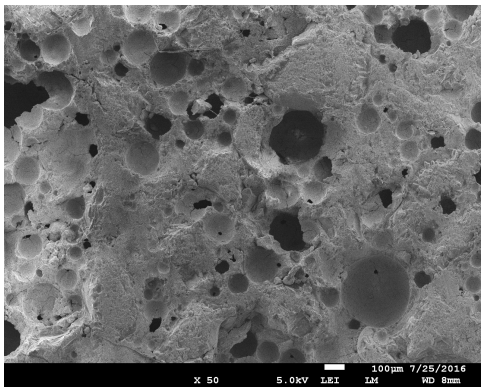

Figure 7.1: SEM measurement of CEMI

most pores are detected 7.1. The surface is generally hydrated due to the grey color. No white crystals are observed, which could be dehydrated grains of grains. This hydration can be water absorbed from the air or moist. When the concrete grows old, the relative portion of dehydrated cores is commonly smaller. However this is a fairly young sample of concrete [19]. From the SEM images it was put forward to use the fractal models to investigate the SESANS measurements, because of the chaotic appearance. Apart from that it was quite difficult to draw useful conclusions from these images. They must be seen as an addition to the SESANS measurements, but a quantitative connection between the two measuring techniques has not yet been made. Some qualitative analysis connecting the two techniques, can be made.
For figure 7.2 the CEMI is viewed at a magnification of 100x. A variety of pore sizes have been detected ranging from 15 microns to 60.9 microns. However even bigger pores can be detected and a range of crystal like formations are also visible. The figure 7.3 shows the SEM image for magnification of 50x for

CEMIII. Here also a wide variety of pore sizes are detected and there appears to be more pores than in the CEMI sample at the same magnification. For figure 7.4 the pore sizes range from 21.8 microns to 55.8 microns, which are smaller in size for magnification of 100x than in CEMI. Also hydrated crystal formations are detected, widely distributed over the surface.

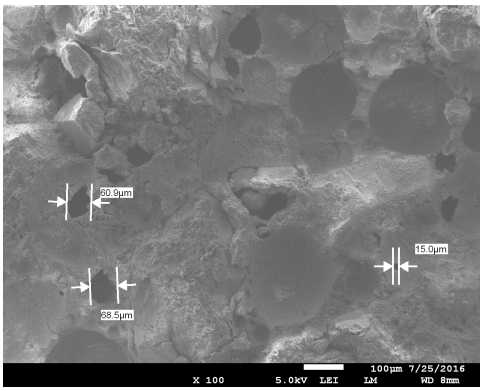

Figure 7.2: SEM measurement of CEMI with length-scales of pores

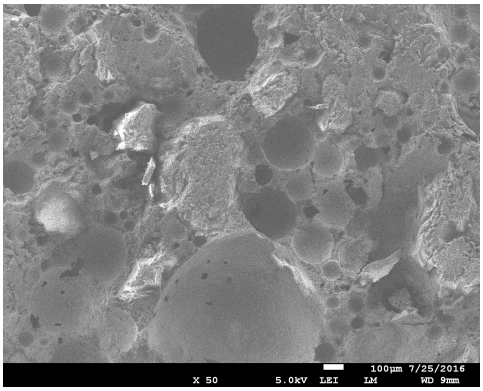

Figure 7.3: SEM measurement of CEMIII/B

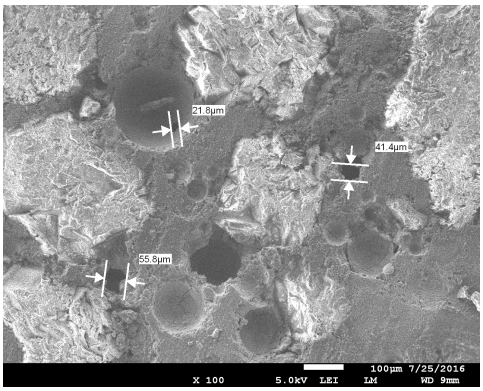

Figure 7.4: SEM measurement of CEMIII with length-scales of pores

There were also a few EDX measurements performed. At the end it was clear that the composition was almost exactly the same at every spot and magnification. The EDX results of CEMI and CEMIII at 50x magnification are presented below. The results are given in graphs to show the different elements peaks at different electron scatter energies. The magnification of the EDX measurements were both at 50x.

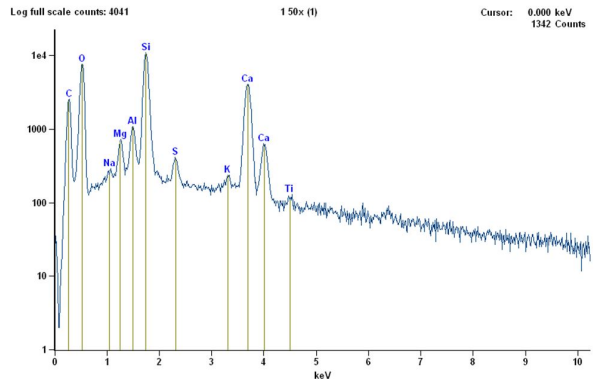

Figure 7.5: EDX measurement of undegraded CEMI

The CEMI sample's composition is almost the same as expected. There wasn't an iron peak (Fe), but actually this peak was manually inserted with the software of the SEM. Noticeable is the fact that the C concentration in the CEMIII is relatively higher than the CEMI. The iron peak of the CEMIII sample can be explained by the blast furnace slag additive. Blast furnace slag is an industrial by-product for production of pig iron from iron ore in blast furnaces. This is mixed into the concrete for more strength and more resistance against dangerous chemicals and makes the concrete less permeable.

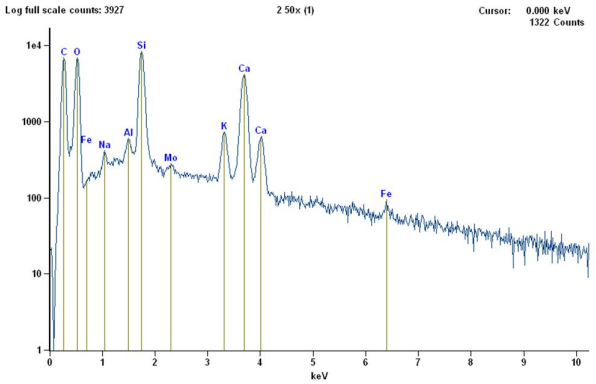

Figure 7.6: EDX measurement of undegraded CEMIII

To know how these elements are distributed and in which form, the XRD measurements were executed. Together with the EDS this explains the compounds and minerals present in the samples. However only for one sample a proper analysis could be performed. This was applicable for the CEMI sample degraded in sulphate for two weeks. The second diffractogram for CEMIII degraded by CO_2 for two weeks was also analysed, but not a complete analysis could be obtained. Two diffractograms are given below.

By using Fulproff it coul be stated that the following compounds were similar with this diffractogram. This is a qualitative analysis for the XRD. For the CEMI sample, which was degraded in sulphate for two weeks, Silicium dioxide SiO_2(s) was found as main component of the sample, which is actually quartz. This compound is not possible to be dissolved in water and is present as a white crystalline powder in the sample. Together with calcite $CaCO_3$(2) these compounds were the solid crystals, which are present in the sample. The calcite was not assumed to be found, because this sample was not degraded by carbonation. However, probably this sample was kept at regular earth's atmosphere condition for a long time until the XRD measurement. This insinuates that the CEMI sample has been carbonated by the carbon dioxide in the air at a lower concentration than the carbonation tank. An idea to stop this

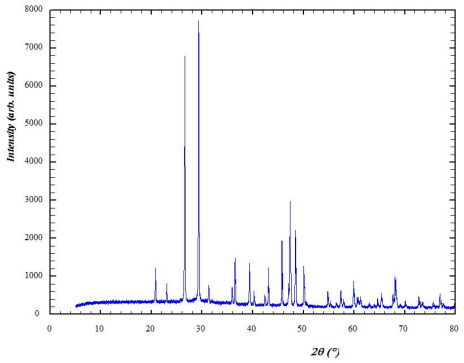

Figure 7.7: XRD pattern of CEMI degraded in sulphate solution for two weeks

process for a follow up experiment, is to keep the sample in a phenolphtalin solution. This stops every degradation process of the sample.
Also gypsum, calcium sulfate $CaSO_4$ was found. Gypsum is formed as a by-product of sulfide oxidation, amongst others by pyrite oxidation, when the sulfuric acid generated (most probable in the solution) reacts with calcium carbonate. Its presence indicates oxidizing conditions. These compounds agree with the elements found with the EDX measurement of the undegraded CEMI, so this is plausible. The Si and O elements were found, so this is correct for the silicium dioxide. Ca, C and O were also found in relatively large quantities, so this is correct for the calcite. It was not expected that regular calciumhydroxide $Ca(OH)_2$ could not be found. This is for ordinary Portland cement quite a big part of its structure. It occupies about 15% of this cement, but it was not found in the XRD pattern. However this result was also obtained by literature [16] with even longer carbonation time, so this is not a mistake. The $Ca(OH)_2$ is most probably converted into calcite $CaCO_3$, which is concluded in Holtzhuizen's Thermogravimetric analysis (TGA). The cause for this is carbonation and dehydration together.
The CEMIII sample was also analysed with the software. This sample was degraded by CO_2 for 2 weeks. The main compound was easily detected, which was also quarts or silicium dioxide SiO_2(s). However not a proper analysis could be made for the second or third compound. This was not expected, because calcite was a compound which was assumed to be in the sample. However, the calcite seemed to be absent in the sample, bcecause the intensity of calcite couldn't match the diffractogram. On top of that, no gypsum was found either in the CEMIII sample, which was also expected to be found. Besides that the problem was that there were too many possible compounds, which could be matched with the diffractrogram. However these matches weren't accurate enough or they would be illogical for the chemistry of the compound. Therefore a second or third compound could not be estimated. The first compound does in fact agree with the EDX measurement.

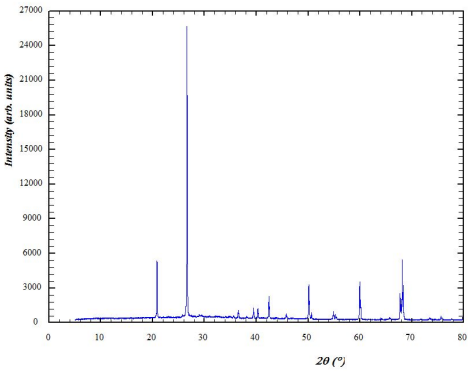

Figure 7.8: XRD pattern of CEMIII/B carbonated for two weeks

8

Conclusion and Recommendations

Several experiments have been performed on concrete to study its porosity and characteristics after degradation. With SESANS the depolarization at different length scales (spin-echo length) were measured. It was concluded that the curves couldn't be analyzed visually, because the saturation of the depolarization could not be exactly pointed out. With two different models the data was analyzed. The Surface Fractal Model and the Infinetely long Cylinder with diameter D was executed. Only the Surface Fractal Model was executed successfully. This way it can be said that concrete has a surface fractal characteristic with decreasing associated lengths for degraded concrete.
It can be concluded that carbonation densifies both CEMI and CEMIII samples. The calcite precipitation causes the pores to get clocked. The pore network gets smaller with carbonation. However, for chloride attack and sulfate ingress the samples are severely affected. The samples become very fragile and even more porous than before. No constructive precipitation and clocking of the pores is analysed. This is concluded from the SESANS data together with the XRD data.
The surface structure and its composition is looked at with SEM. It showed the porosity at different magnification levels, which indicated that nano-pores weren't as visible as expected. Pores at a micrometer scale were way more likely to be observed. With EDX the composition of the surfaces were measured. It was obvious that both CEMI and CEMIII consisted mostly out of the elements C, O, Si and Ca. Apart from these basic concrete elements a few other salts are found in the concrete, such as Na and Al. The iron element in CEMIII comes from the blast furnace slag addition.
Analysis with XRD showed the basic compounds of two samples after degradation. The main compound was clear, which was quarts. Also precipitation in the carbonated sample, such as calcite was present, and also gypsum for the degraded sample by sulfates was analysed. These compounds agreed with the EDX analysis, because the elements matched the different compounds. Although these compounds were gained, the analysis of the XRD is a difficult task, which wasn't successful for all samples. It is recommended that more analysis is performed to connect the SESANS and SEM measurements. Now only the different techniques are discussed separately, but a connection between the two results should be more carefully investigated. Other measuring techniques should also be used to obtain more insight on the porosity of the concrete, because this way more scales of the concrete can be visualized and interpreted. Proposed techniques are SANS and USANS. Some of these techniques are available at the TU Delft, others should be obtained elsewhere.
Besides that, more samples should be researched to acquire a bigger data-set for a more reliable and well-grounded research. The CEMI and CEMIII could be degraded at different time scales and the results should be compared. Eventually more conclusions can be drawn from more measurements, which will gain the knowledge about the concrete. For the analysis, there are also way more models to consider to fit the data of the SESANS. Concrete has quite a complicated structure as seen in the SEM measurements (and this is only the surface), so this means many kinds of characteristic geometry models can be fitted to the SESANS data. In this research only two models were used and the visual analysis was not even applicable. With SESANS it is also a possibility to combine models, in which there are even more situation to be described. The idea is to find the best fit for the data, which gives the best explanation for the structure and porosity in the concrete.
Next to gain more insight on the surface structure and how this changes after degradation, it is advised

that the concrete samples (both CEMI and CEMI) are measured with SEM again after degradation. This way a the results can be compared and more conclusions can be drawn from the change of concrete through degradation. Different time scales for degradation can be used obtain accurate knowledge of how the concrete changes with longer periods of degradation. This should happen for all the deterioration processes, so for the carbonation, sulfide attack and chloride attack. It is disappointing that the SEM measurements are quite expensive, so this plan has to be thought through before the start, so no money is wasted on unnecessary measurements.
For the SESANS data analysis, the model for the Infinitely long Cylinder with diameter D should be extended and completed to fit the existing data. To write the code for this model takes a long time, so this is a possible follow-up research, which can be executed by another Bachelor student. It is still very favourable to use this model, because this curve is very similar to the curves obtained by the SESANS measurements. This makes it a possible geometry for the concrete pores in these environments.
The XRD measurements could also be more expanded and the analysis should be more thorough to find the exact compounds. The other samples should also be measured with XRD to broaden the data for comparison.
Another addition to the degradation analysis of the samples is to monitor the different ions present in the solutions. Equipment is available at the RID for this to keep record of the concentration of Na^{+}, Cl^{-} and Ca^{2+}. This could give more insight to the progress during the degradation.

Bibliography

[1] E. Verhoef, E. Neeft, G. Deissmann, R. Wiegers, and D. Kers, *Waste families in opera,* (2016).

[2] R. Andersson, L. Van Heijkamp, I. De Schepper, and W. Bouwman, *Analysis of spin-echo small-angle neutron scattering measurements,* Journal of Applied Crystallography **41**, 868 (2008), cited By 38.

[3] E. V. Verhoef, A. de Bruin, R. Wiegers, E. Neeft, and G. Deissmann, *Cementitious materials in opera disposal concept in boom clay,* OPERA-PG-COV020 (2014).

[4] S. Hemes, G. Desbois, J. L. Urai, B. Schröppel, and J.-O. Schwarz, *Multi-scale characterization of porosity in boom clay (hades-level, mol, belgium) using a combination of x-ray μ-ct, 2d bib-sem and fib-sem tomography,* Microporous and Mesoporous Materials **208**, 1 (2015).

[5] W. Kraan, V. Zabenkin, Y. Chetverikov, M. Rekveldt, C. Duif, and S. Grigoriev, *Multiple scattering in magnetic {SESANS},* Physica B: Condensed Matter **397**, 79 (2007), proceedings of the Sixth International Workshop on Polarised Neutrons in Condensed Matter Investigations.

[6] Z. Zhou, W. Bouwman, H. Schut, S. Desert, J. Jestin, S. Hartmann, and C. Pappas, *From nanopores to macropores: Fractal morphology of graphite,* Carbon **96**, 541 (2016), cited By 3.

[7] P. W. Schmidt, *Small-angle scattering studies of disordered, porous and fractal systems,* Journal of Applied Crystallography **24**, 414 (1991).

[8] D. F. R. Mildner and P. L. Hall, *Small-angle scattering from porous solids with fractal geometry,* , 1535 (1986).

[9] P.-J. C. J. J. Coumou, A. M. A. Brizard, J. H. van Esch, I. M. de Schepper, and W. G. Bouwman, *Spin-echo small-angle neutron scattering (sesans) measurements of needle-like crystallites of gelator compounds,* Journal of Physics: Conference Series **251**, 012035 (2010).

[10] X.-S. Wang, B.-S. Wu, and Q.-Y. Wang, *Online {SEM} investigation of microcrack characteristics of concretes at various temperatures,* Cement and Concrete Research **35**, 1385 (2005).

[11] D. B. Williams and C. B. Carter, *The transmission electron microscope,* in *Transmission electron microscopy* (Springer, 1996) pp. 3–17.

[12] R. Chaïd, S. Kenaï, H. Zeroub, and R. Jauberthie, *Microstructure and permeability of concrete with glass powder addition conserved in the sulphatic environment,* European Journal of Environmental and Civil Engineering **19**, 219 (2015), cited By 0.

[13] E. Verhoef and E. Neeft, *Outline of a disposal in clay,* (2014).

[14] C. Xiong, L. Jiang, Y. Xu, H. Chu, M. Jin, and Y. Zhang, *Deterioration of pastes exposed to leaching, external sulfate attack and the dual actions,* Construction and Building Materials **116**, 52 (2016).

[15] V. Zivica and A. Bajza, *Acidic attack of cement based materials — a review.: Part 1. principle of acidic attack,* Construction and Building Materials **15**, 331 (2001).

[16] P. Holthuizen, *Chloride ingress of carbonated blast furnace slag cement mortars,* Master Thesis (2016), uuid:adda67de-f31e-4380-91c3-67a3a29e0b95.

[17] K. Kobayashi, K. Suzuki, and Y. Uno, *Carbonation of concrete structures and decomposition of c□s□h,* Cement and Concrete Research **24**, 55 (1994).

[18] S. Diamond, *The microstructure of cement paste and concrete—a visual primer,* Cement and Concrete Composites **26**, 919 (2004), scanning electron microscopy of cements and concretes.

[19] H. M. Jennings, J. J. Thomas, J. S. Gevrenov, G. Constantinides, and F.-J. Ulm, *A multi-technique investigation of the nanoporosity of cement paste,* Cement and Concrete Research **37**, 329 (2007), cementitious Materials as model porous media: Nanostructure and Transport processesJuly 2005, Centro Monte Verita, Switzerland.